JMEPEG (2009) 18:129–136
DOI: 10.1007/s11665-008-9243-3

1059-9495/$19.00

The Effect of Inhibitors on the Susceptibility of Al 6013/SiC Interface to Localized Corrosion

Zaki Ahmad and B.J. Abdul Aleem

(Submitted July 26, 2006; in revised form March 14, 2008)

Al 6013-20 SiC (p) in tempers T4, O, and F is sensitive to localized corrosion in 3.5 wt.% NaCl because of the preponderance of the secondary phase particles of Cu, Fe, and Cr at the Al/SiC interface. Treatment with cerium chloride effectively inhibited the localized corrosion of the alloy by suppressing the cathodic reactions at Al 6013/SiC interface as shown by electrochemical investigations. Morphological studies showed the formation of a protective cerium oxide/hydroxide films, which suppresses the corrosion of the alloy.

Keywords Al/SiC interface, corrosion potential, corrosion rate, inhibition, intermetallics, pitting potential, polarization, metal matrix composites

1. Introduction

Considerable work has been devoted to aluminum metal matrix composites due to the need for economically compatible materials with high specific strength and stiffness. Discontinuously reinforced aluminum (DRA) composites, composed of high strength alloys reinforced with SiC particles, possess an excellent combination of superior mechanical properties such as high specific elastic modulus, high specific yield strength, and wear resistance. They can be produced with isotropic properties using conventional secondary fabrication methods making them relatively inexpensive compared to composites reinforced with continuous filaments. Al alloys 6061 and 6013 reinforced with silicon carbide are the focus of attention because of their combination of superior mechanical strength and wear and corrosion resistance. The 6xxx series of aluminum alloys exhibited a superior resistance to corrosion; however, their mechanical properties are lower compared to other age-hardenable alloys (Ref 1-3).

To overcome the above limitation, Al-Mg-Si alloys were developed, which showed improved mechanical strength and hardness (Ref 4-6). Al alloys used in composites are generally commercial Al 2024, 7075, 5156, and 6061 alloys (Ref 7-9). Al 6013 reinforced with 20% SiC (p) was a late entry in the market; however, it became the focus of attention because of its suitability for structural applications where high strength, high modulus, and ductility are required. It rivaled the advantages offered by Al 2024 once widely employed for aerospace applications and patented by Alcoa.

Zaki Ahmad and **B.J. Abdul Aleem**, Mechanical Engineering Department, King Fahd University of Petroleum and Minerals, Dhahran, Saudi Arabia. Contact e-mails: ahmadz@kfupm.edu.sa and abaleem@kfupm.edu.sa

Particle reinforced Al/Sic metal matrix composites such as Al 6013-20 SiC (p) exhibit improved mechanical and physical properties compared to wrought alloys; however, they are more susceptible to pitting than their monolithic counterparts (Ref 10-12). They also exhibit a high corrosion rate at velocities higher than 2.3 m/s as shown by an earlier work (Ref 13). Recent work on Al 6013-20 SiC (p) showed its sensitivity to pitting and erosion corrosion in sodium chloride solution flowing at velocity ranging from 1 to 3.8 m/s (Ref 13, 14). A variety of surface modification methods such as anodizing, chromate conversion coatings, organic finishings have been suggested for the protection of aluminum metal matrix composites from localized corrosion (Ref 15-17). Despite the advantages offered by chromate conversion coatings, their application has been limited because of recognized health risks associated with them. Cerium coatings have been the focus of attention in recent years (Ref 18-20). It has been reported that cerium rich coatings suppressed the corrosion of Al 7075 in 3.5 wt.% NaCl (Ref 18, 19). Sodium molybdate treatment has also been suggested for Al metal matrix composites. Work on the corrosion inhibition of Al 6013-20 SiC (p) has not been reported earlier in literature. This paper describes the effectiveness of cerium chloride and sodium molybdate treatment on the corrosion inhibition of Al 6013-20 SiC (p) in neutral sodium chloride solutions.

2. Experimental

2.1 Material

The atomized material powder of Al 6013 and 15 μSiC reinforcement (20 vol.%) were blended and compacted under controlled conditions. Following consolidation with billets (25.4 cm dia) they were forged and finally rolled to a thickness of 2.5 mm. The alloy was annealed for 3 h to obtain temper O, solution treated at 525 °C for 30 min, water quenched, and naturally aged to obtain temper T4. The alloy obtained after rolling without any heat treatment was designated as temper F. The alloy was produced by VAW Aluminum AG, Germany.

Al6013-20 SiC (p) alloy in tempers, O (annealed for 3 h and furnace cooled), F (as fabricated), and T4 (solution treated at

Table 1 Nominal composition of alloy Al 6013[a]

Si	Fe	Cu	Mn	Mg	Cr	Zn	Ti	Balance
0.6-1.0	0.5	0.6-1.0	0.2-0.8	0.8-1.2	0.1	0.25	0.1	Aluminum

[a]The alloy was blended with 20 vol.% SiC particulates

525 °C for 30 min, water quenched, and naturally aged) was used for investigations. The chemical composition of the matrix Al 6013 is given in Table 1.

The manufacturer of the alloy was VAW Aluminum Ag, Research Development Company, Germany. The alloy was blended with 1.5 μsilicon carbide particulate reinforcement.

2.2 Experimental Procedures

2.2.1 Weight Loss Studies. Weight loss studies were conducted in accordance with ASTM specifications G31-72 (Ref 21). Specimens in triplicate were exposed to 3.5 wt.% NaCl for 500 h at 25 ± 2 °C. The solution was smoothly stirred. Corrosion rates were calculated in units of mpy (mils/year) and mdd (milligrams/decimeter square/day). The corroded specimens were dried overnight before being weighed to determine the loss in weight after exposure. The studies were conducted under open air conditions. All solutions were stirred slowly during the exposure period.

2.2.2 Electrochemical Polarization Plots. *Tafel Plots.* Potentiodynamic polarization measurements were made in accordance with ASTM standard specification, G-89 (Ref 22). Specimens were immersed in 3.5 wt.% NaCl solution for 3 h prior to polarization. The solution was purged with nitrogen for 45 min prior to commencement of polarization. Polarization was commenced from the corrosion potential (E_{corr}), first in the cathodic direction up to −1300 mV_{SCE} and later in the anodic direction up to −300 mV_{SCE}. The scan rate was 10 mV/min. A potentiodynamic measurement system fitted with a microprocessor was used for polarization. After immersion for 1 h, experiments were performed by applying a controlled potential over a small range (±30 mV vs SCE) with respect to E_{corr}. A scan rate of 1 mV/min was used. The values of β_a and β_c were predetermined from potentiodynamic curves. A software (softcorr 350) capable of performing five different electrochemical techniques was used to plot the curves and obtain the corrosion rates from the electrochemical data generated. Polarization resistance experiments were conducted in accordance with the ASTM G-59-91 practice (Ref 23). The solution was continuously agitated by a stirrer in the cell.

2.2.3 Cyclic Polarization Measurements. All measurements were made in accordance with ASTM standard G 61-78 (Ref 24). The potential was allowed to stabilize for 45 min prior to the commencement of polarization. Polarization was reversed after reaching a current density of 100 $\mu A/cm^2$. Pitting potential E_p was indicated by a sudden rise in the anodic polarization curve. The scan rate was maintained at 1 mV/s. The solution was purged with nitrogen prior to commencement of polarization and stirred continuously.

2.2.4 Recirculation Loop. A recirculating loop made from high density polyvinyl chloride (HDPVC) was used to study the effect of velocity on corrosion. A continuous circulation system was maintained in the loop. The water entered through a control valve into the specimen chambers with varying diameters. The water left the loop through an exit valve and re-entered the closed circulation tank. A centrifugal pump of capacity 20 m^3/h was used. Devices such as magnetic flow meter, pH sensors, temperature recorder, and conductivity meter were installed in the system. The pH of the solution was constantly adjusted to 7-8. Specimens in triplicate for each condition were introduced in the specimen holder for 168 h. A temperature of 40 ± 2 °C was maintained in the PVC recirculating loop. The solution in the tank was not treated with nitrogen.

Table 2 Comparison of corrosion rate of Al 6013-20 SiC (p) in 3.5 wt.% NaCl in the presence of 1000 ppm $K_2Cr_2O_7$ + 1000 ppm $NaHCO_3$ as inhibitor (open air condition) at 25 ± 2 °C

		Corrosion rate			
		3.5 wt.% NaCl + 0 inhibitor		3.5 wt.% NaCl + inhibitor	
Alloy designation	Velocity, m/s	mpy	mdd	mpy	mdd
Al 6013-20 SiC (p)-O	1	11.8	22.1	3.07	5.76
	1.9	11.6	21.7	7.63	14.32
	2.7	12.9	24.2	8.4	15.77
	3.8	13.6	25.5	9.63	18.08
Al 6013-20 SiC (p)-F	1	9.9	18.5	3.01	5.65
	1.9	10.4	19.5	4.31	8.09
	2.7	10.8	20.2	5.53	10.38
	3.8	11.3	21.2	6.6	12.39
Al 6013-20 SiC (p)-T4	1	9.6	18	2.01	3.77
	1.9	10.1	18.9	2.7	5.07
	2.7	10.8	20.2	3.4	6.38
	3.8	11.4	21.4	3.8	7.13

2.2.5 Electron Microscopy and Microanalytical Studies. All studies were conducted in a low vacuum scanning electron microscope (LVSEM). In this system, an additional pumping system is added to maintain the specimen chamber in low vacuum when the column is still in a high vacuum. A microanalysis system with a Quant mapping software package for X-ray mapping was used for Energy Dispersive Studies (EDS).

2.2.6 Inhibitors. The following inhibitor solutions were prepared.

(a) 1000 ppm $K_2Cr_2O_7$ + 1000 ppm $NaHCO_3$ + 3.5 wt.% NaCl.
(b) 1000 ppm Cerium Chloride + 3.5 wt.% NaCl.
(c) 1000 ppm Sodium molybdate + 3.5 wt.% NaCl.

2.3 Surface Treatment

All samples were ground successively with 240, 320, 400, and 600 grit SiC paper. Samples for microstructural studies were also polished with a 6 micron diamond paste. Corrosion tests were conducted in 3.5 wt.% NaCl, 100 ppm $K_2Cr_2O_7$ + 1000 ppm $NaHCO_3$ + 3.5 wt.% NaCl, 1000 ppm cerium chloride + 3.5 wt.% NaCl, and 1000 ppm Sodium molybdate + 3.5 wt.% NaCl.

3. Results and Discussion

The results of inhibition studies on tempers O, T4, and F of alloy 6013 are summarized in Table 2.

As shown by Table 2, the corrosion rates of all tempers increase with an increase in velocity both in the presence and absence of inhibitors. Temper O exhibits higher corrosion rate after inhibition treatment compared to tempers F and T4. At the highest experimental velocity (3.8 m/s), the corrosion rates of tempers F and T4 decrease from 11.3 mpy and 11.4 mpy to 6.6 mpy and 3.8 mpy, respectively. The significant reduction in corrosion rates under dynamic flow observed in the investigations signifies the effectiveness of $K_2Cr_2O_7$-$NaHCO_3$ mixture as an effective inhibitor. The reduction in the corrosion resistance of Al 6013-20SiC (p) with increased velocities may be attributed to the lack of ductility of matrix caused by the larger volume of reinforcing particles (Ref 25) and by continuous removal of protective layer by the erodent particles. The protrusion of particulates on the surface also makes it difficult to achieve a passivating layer, which lowers the resistance to corrosion with increased velocity.

The reduction in corrosion rate of the alloy may be attributed to the formation of a protective layer of boehmite ($Al(OH)_3 \cdot 3H_2O$) and bayrite ($Al_2O_3 \cdot 3H_2O$) (Ref 13). Higher velocities lead to the breakdown of these protective layers which lead to pitting on the alloy surface. The breakdown of the oxide layer leading to pitting of Al 6013-20 SiC (T4) in 3.5 wt.% NaCl at a velocity of 2.7 m/s is shown in Fig. 1. A pit at a higher magnification is shown in Fig. 2. The formation of the protective boehmite layer ($Al(OH)_3 \cdot 3H_2O$) was clearly established by F.T.I.R. (Fourier Transformation Infrared Spectroscopy) in an earlier study (Ref 26). At higher velocities (3.8 m/s), some free SiC particles were observed to be dislodged as shown in Fig. 3. In Al-SiC composites, the rate of corrosion is observed to be higher compared to matrix alloy, and SiC/Al interface is the preferred site for localized corrosion. The site is abundantly located with copper intermetallics as reported by the authors earlier (Ref 26). The secondary phase precipitates mostly of copper are abundantly populated at the interface, which promotes the localized corrosion of composite (Ref 26). The existence of high thermal stresses and dislocation densities at the interface also affects the kinetics of erosion corrosion (Ref 27, 28) and increases the sensitivity of the alloy to erosion corrosion. The $K_2Cr_2O_7$-$NaHCO_3$ mixture is an effective inhibitor, as shown by the significant reduction in the corrosion rates of the alloy (Table 2). However, due to the toxic nature of $K_2Cr_2O_7$, further investigations were conducted with cerium chloride (Ref 29) and sodium molybdate (Ref 30) which are nontoxic.

3.1 Effect of $CeCl_3$ and $NaMoO_4$

Because of the encouraging results obtained by cerium chloride and sodium molybdate treatment of Al 7075 and Al 1100, the investigations were undertaken to observe the effect of the above inhibitors on Al 6013-20 SiC (29-30). The weight loss studies were further substantiated by electrochemical studies. The results of weight loss studies on the effect of $CeCl_3$ and $NaMoO_4$ on the corrosion inhibition of the three tempers of Alloy Al 6013-20 SiC (p) at 50, 70, and 100 °C are summarized in Table 3.

The maximum effect of inhibition is observed on temper T4 of the alloy in both $CeCl_3$ and $NaMoO_4$. The effect of inhibitors on suppressing the corrosion rate is clearly observed in all tempers in Table 3. Cerium chloride is a more effective inhibitor than sodium molybdate as shown by a larger reduction in the corrosion rates brought by the addition of cerium chloride. The corrosion rate of temper T4 decreases from 19.13 to 3.96 mpy on treatment with cerium chloride at 100 °C compared to 10.15 mpy with sodium molybdate.

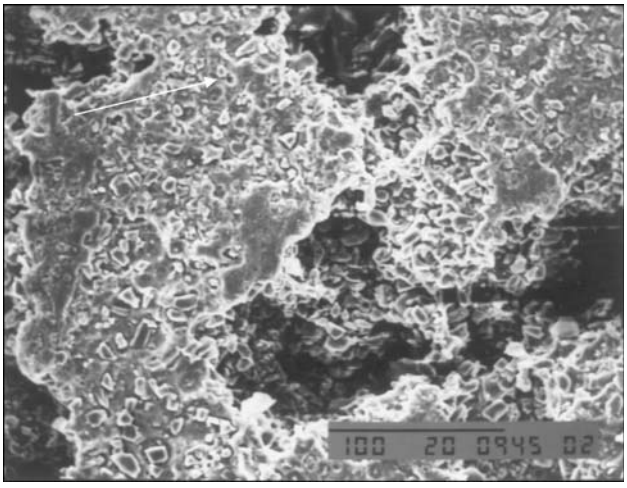

Fig. 1 Breakdown of the oxide layer and pitting on Al 6013-20 SiC (p)-T4 surface at a velocity of 2.7 m/s

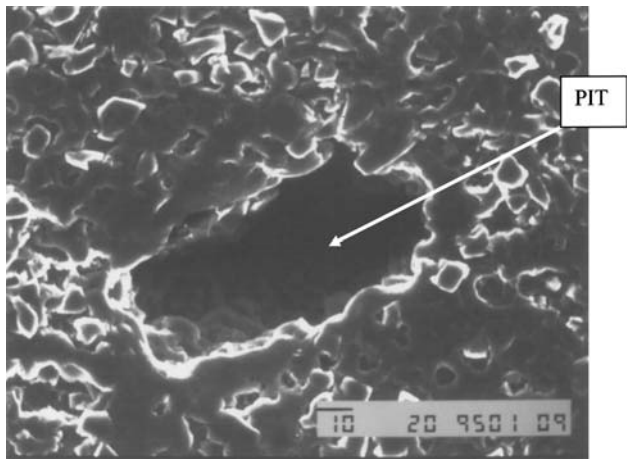

Fig. 2 A pit in Fig. 1 shown at a higher magnification

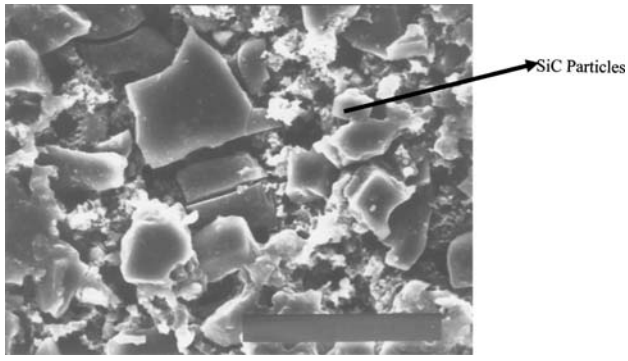

Fig. 3 Some dislodging of SiC particles of Al 6013-20 SiC (p)-O at 3.8 m/s

Table 3 Effect of $CeCl_3$ and $NaMoO_4$ on the corrosion inhibitor of different tempers of Al 6013-20 SiC in 3.5 wt.% NaCl at temperature 50-100 °C (solution in contact with open air and stirred slowly)

			Corrosion rate					
			3.5 wt.% NaCl		3.5 wt.% NaCl + 1000 ppm $CeCl_3$		3.5 wt.% NaCl + 1000 ppm $NaMoO_4$	
Sl. No.	Temperature, °C	Temper	mpy	mdd	mpy	mdd	mpy	mdd
1	50	O	4.72	8.86	1.24	2.32	3.8	7.13
		F	2.20	4.13	1.92	3.6	1.8	3.38
		T4	1.71	3.21	0.472	0.88	0.9	1.69
2	70	O	8.3	15.5	2.73	5.12	5.06	9.5
		F	6.53	12.26	2.16	4.05	4.01	7.53
		T4	2.54	4.77	0.74	1.38	2.01	3.77
3	100	O	12.9	24.2	8.6	16.15	8.05	15.11
		F	11.6	21.7	6.5	12.2	8.21	15.41
		T4	10.19	19.13	3.96	7.43	5.41	10.15

Table 4 Effect of (a) Cerium chloride and (b) sodium molybdate on the inhibition of Al 6013-20 SiC (p) in 3.5 wt.% NaCl (deaerated) (polarization resistance studies) at 25 ± 2 °C

						Corrosion rate	
Sl. No.	Temperature, °C	Temper	R_p, K-ohms	E_{corr}, mV	I_{corr}, μA/cm^2	mpy	mdd
(a) Cerium chloride							
1	50	O	4.004	−0.8	3.727	1.60	2.99
		F	3.301	−0.783	6.57	2.82	5.28
		T4	2.43	−0.791	1.1	0.47	0.88
2	70	O	1.281	−0.909	4.757	2.04	3.81
		F	9.14	−0.915	3.933	1.68	3.14
		T4	10.07	−0.993	2.155	0.92	1.73
3	100	O	1.2	−0.87	17.98	7.71	14.42
		F	1.43	−0.868	15.17	6.50	12.16
		T4	1.53	−0.941	9.2	3.94	7.37
(b) Sodium molybdate							
1	50	O	44.5	−0.8	150	1.24	3.22
		F	11.91	−0.716	211.5	1.92	3.60
		T4	41.3	−0.791	72.8	0.47	0.88
2	70	O	58.57	−0.909	272.6	2.74	5.11
		F	23.76	−0.916	127	2.17	4.06
		T4	34.87	−0.867	111.5	0.75	1.40
3	100	O	100	−0.87	100	8.60	16.08
		F	100	−0.868	100	6.50	12.16
		T4	58	−0.947	74	3.96	7.41

Abbreviations: E_{corr} = Corrosion potential; I_{corr} = Corrosion current; R_p = Polarization resistance

Electrochemical studies were also conducted to evaluate the effect of the inhibitors on the corrosion resistance of Al 6013 in tempers O, F, and T4. The results of electrochemical studies are summarized in Table 4.

The electrochemical studies clearly establish that cerium chloride is a more effective inhibitor. Increased polarization resistance (R_p) is shown by temper T4 of the alloy in both $CeCl_3$ and $NaMoO_4$ as shown by the results. Slightly lower values of corrosion rates are exhibited by all the three tempers of the alloy at 50, 70, and 100 °C in cerium chloride compared to sodium molybdate. The inhibitor effectiveness, however, decreases with an increase in temperature. The effect of inhibition on electrochemical parameters E_{corr} and E_p is shown in Table 5. The electrochemical parameters E_p (pitting potential) and E_{corr} (corrosion potential) were obtained from cyclic polarization curves.

The difference between E_{corr} and E_p is taken as an indicator of pitting resistance, the lesser the difference, the lesser the resistance. The difference between E_p and E_{corr} is very small in sodium chloride and it indicates a lesser resistance to corrosion in the absence of inhibitor as shown in Table 5. The corrosion potential of all tempers shifts closer to E_p in 3.5 wt.% NaCl and the tempers show a sensitivity to pitting. The larger difference on the other hand, between E_{corr} and E_p, gives a measure of the effectiveness of cerium chloride as an effective cathodic inhibitor. This difference exhibited by temper T4 is maximum (−160 mV_{SCE}) at 25 °C, and it tends to decrease with increasing temperature. A cathodic polarization curve of temper T4 of the alloy in 3.5 wt.% NaCl + 100 ppm $CeCl_3$ is shown in Fig. 4. The cathodic polarization curves obtained in 3.5 wt.% NaCl, 3.5 wt.% NaCl + 1000 ppm $CeCl_3$, and 3.5 wt.%

Table 5 Effect of addition of $NaMoO_4$ and $CeCl_3$ on the pitting potential (E_p) and corrosion potential (E_{corr}) of different tempers of alloy 6013-20 SiC (p) in 3.5 wt.% NaCl (deaerated conditions) at 25 ± 1 °C

			3.5 wt.% NaCl		3.5 wt.% NaCl + 1000 ppm $CeCl_3$		3.5 wt.% NaCl + 1000 ppm $NaMoO_4$	
Sl. No.	Temperature, °C	Temperl	E_{corr}, mV	E_p, mV	E_{corr}, mV	E_p, mV	E_{corr}, mV	E_p, mV
1	25	T4	−670	−650	−750	−590	−615	−510
2	50	T4	−700	−680	−796	−706	−630	−520
		F	−780	−750	−780	−720	−630	−650
		O	−790	−770	−800	−750	−635	−540

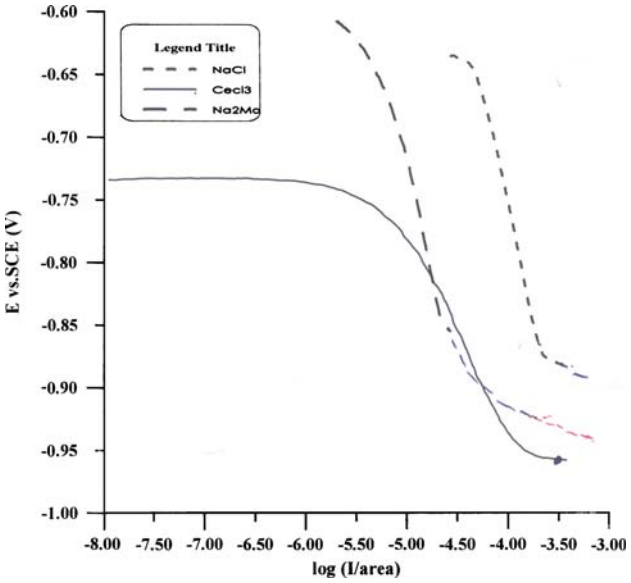

Fig. 4 A cathodic polarization curve of temper T4 of the alloy in 3.5 wt.% NaCl + 1000 ppm $CeCl_3$ in deaerated condition

Table 6 Effect of Addition of $NaMoO_4$ and $CeCl_3$ on the corrosion current density of Al 6013-20SiC (p)-T4 (deaerated conditions) at 25 ± 2 °C

Sl. No.	Media	I_{corr}, μA/cm^2
1	3.5 wt.% NaCl	234
2	3.5 wt.% NaCl + 1000 ppm $CeCl_3$	25.1
3	3.5 wt.% NaCl + 1000 ppm $NaMoO_4$	178

NaCl + 1000 ppm $NaMoO_4$ are overlaid on the main curve as shown in the figure. The maximum reduction in current density (from 234 to 25.1 μA/cm^2) is exhibited by temper T4 in cerium chloride. The current densities recorded in the investigations are summarized in Table 6. A comparison of the corrosion rates of three tempers of the alloy based on Tafel analysis is shown in Fig. 5(a-c).

Based on the above evidence, cerium chloride acts as a strong cathodic inhibitor for the alloy. Sodium molybdate on the other hand is an anodic inhibitor, which acts by raising the E_p in the positive direction while maintaining E_{corr} negative to E_p. The anodic polarization curve shifts in the positive direction. A typical cyclic polarization curve of T4 temper of the alloy in 3.5 wt.% NaCl + 1000 ppm $NaMoO_4$ is shown in Fig. 6. The corrosion potential of the alloy tends to shift to

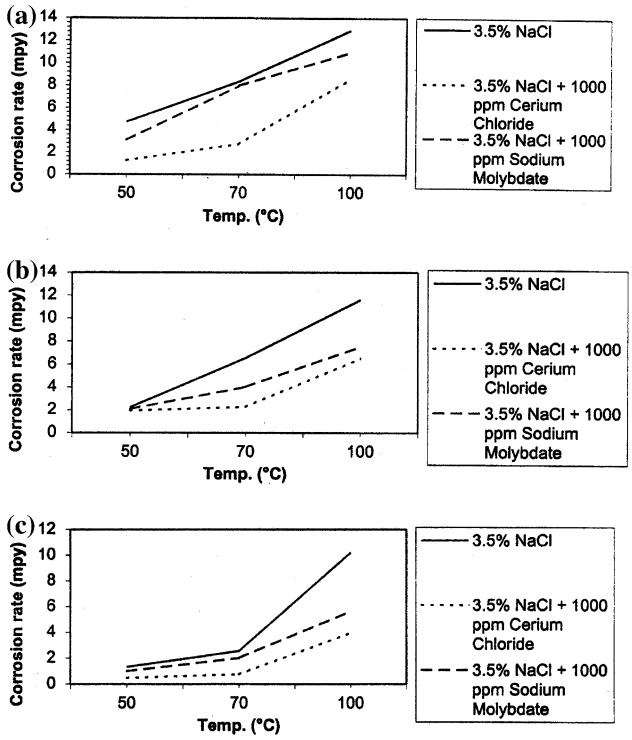

Fig. 5 (a) Comparison of corrosion rates of Al 6013-20 SiC (p)-O by Tafel Analysis in deaerated condition. (b) Comparison of corrosion rates of Al 6013-20 SiC (p)-F by Tafel Analysis in deaerated condition. (c) Comparison of corrosion rates of Al 6013-20 SiC (p)-T4 by Tafel Analysis

more positive values of potential, which shows that it is an anodic inhibitor.

3.2 Effect of $CeCl_3$ and $NaMoO_4$ Inhibitor on Surface Morphology

There is no sufficient published information on the kinetics and mechanism of corrosion behavior of Al-Si MMCs by Ce_2O, $Al(OH)_3$, $Al_2O_3 \cdot 3H_2O$, $Al_2O_3 \cdot H_2O$ films on Al MMCs (Ref 27, 30-32). The evidence on the effect of cerium ions on the aluminum oxide/hydroxide protective films in the studies presented is qualitative, although not conclusive. The surface morphology of Al 6013 - SiC (p) in 3.5 wt.% NaCl containing 1000 ppm $CeCl_3$ is shown in Fig. 7. The micrograph reveals the formation of blisters of circular shape. Two types of particles cerium oxide and aluminum oxide are observed. The blisters contain both cerium oxide/hydroxide and aluminum

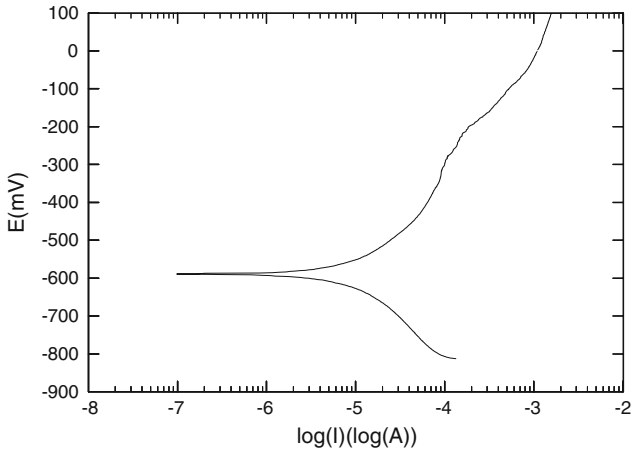

Fig. 6 A typical cyclic polarization curve of Al 6013-20 SiC (p)-T4 temper of the alloy in 3.5 wt.% NaCl + 1000 ppm sodium molybdate in deaerated conditions

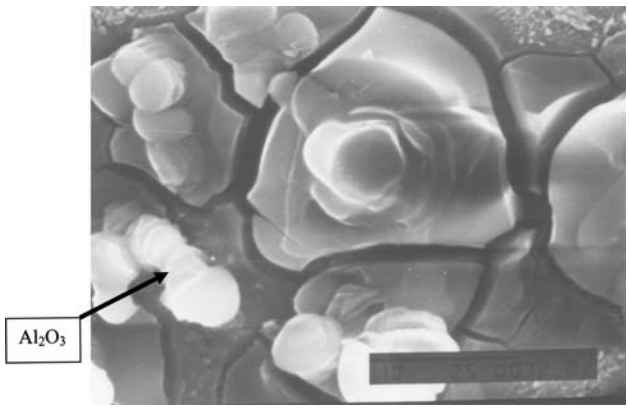

Fig. 7 Surface morphology of Al 6013-SiC (p) in 3.5 wt.% NaCl containing 1000 ppm $CeCl_3$

oxide/hydroxide. The concentration of Al_2O_3 is predominant in the blisters. Electron micrograph studies by other workers on Al 7075 were inconclusive and the particles of Al_2O_3 could not be bench marked (Ref 18). The deposition of two types of particles in concentric rings is shown in Fig. 8. The square shaped particles of cerium oxide identified by EDS studies are shown in Fig. 9. Figure 10 shows the oxide layers containing CeO_2 and Al_2O_3 particles. Once the oxide layer thickens, it flakes off. The broken oxide layer in the form of blisters (mothballs) is shown in Fig. 11. The coatings exhibit cracking (mud cracking) after longer exposure time in air due to drying of the gel as shown in Fig. 12. It has been conclusively shown by the investigations presented above that cerium chloride and sodium molybdate inhibits the corrosion of different tempers of Al 6013-20 SiC (p) in sodium chloride solution at ambient and elevated temperatures. Mechanism of corrosion on Al/SiC composites is inconclusive. In earlier studies, it was reported that pits initiate on copper intermetallics, which are formed preferentially at the SiC/Al surface (Ref 12). In a corrosion studies by the authors on Al 6013-20 SiC (p), it was qualitatively established that the SiC/Al interface is the preferred location for the intermetallics of copper, which has a more positive potential than Al matrix, and hence the

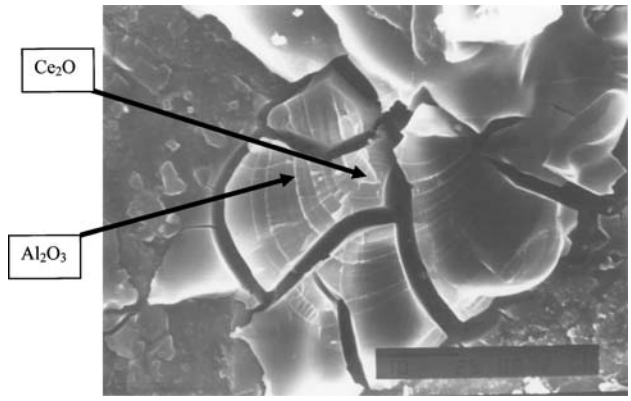

Fig. 8 Deposition of two types of particles (cerium + aluminum) on Al 6013-20 SiC (p)

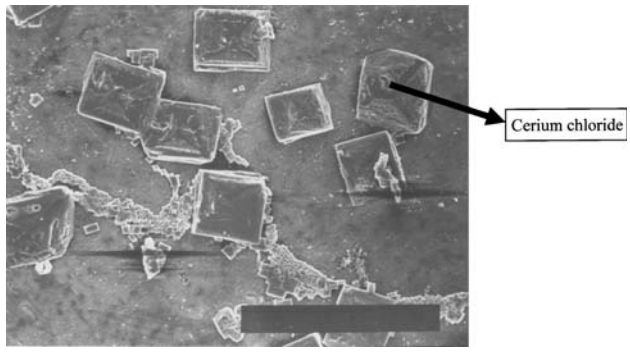

Fig. 9 Square-shaped particles containing predominantly cerium chloride formed on cathodic polarization

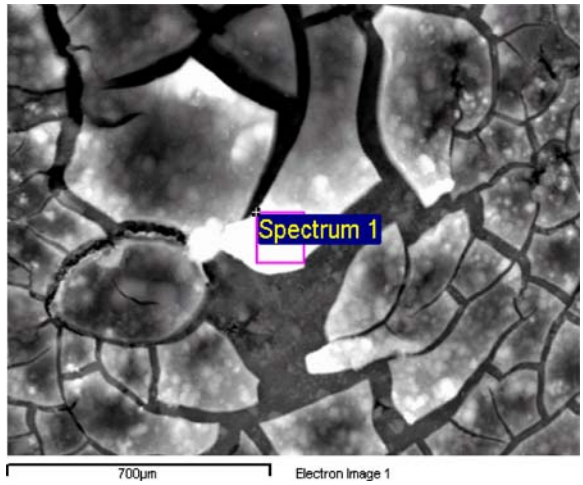

Spectrum	C	O	Al	Si	P	Cu	Ce	Total
Spectrum 1	1.17	59.67	25.69	11.64	0.53	0.95	0.35	100.00
Max.	1.17	59.67	25.69	11.64	0.53	0.95	0.35	
Min.	1.17	59.67	25.69	11.64	0.53	0.95	0.35	

All results in Weight Percent

Fig. 10 Cracked oxide layer containing mixed CeO_2 and Al_2O_3 particles

interface is sensitive to attack by corrosion due to galvanic current (Ref 27). It was shown also by TEM studies that the generations of dislocations at the interface make the interface

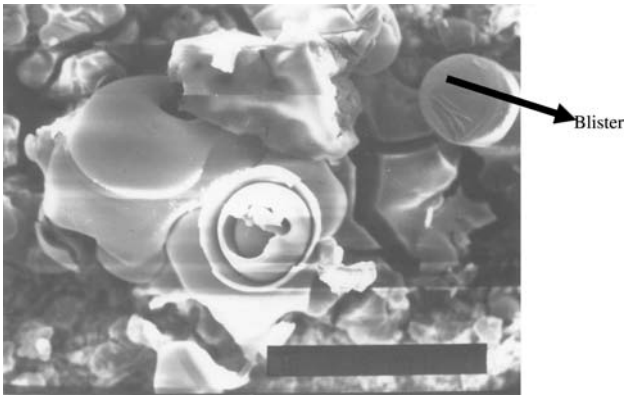

Fig. 11 Broken oxide layer forming blisters (mothballs)

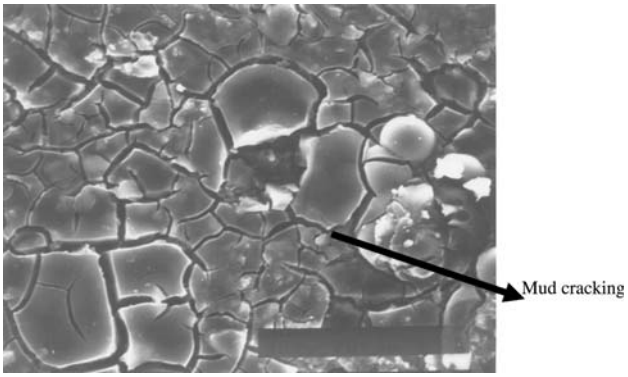

Fig. 12 Mud cracking due to drying of gel after exposure to open air

more reactive (Ref 27). The reduction in the rate of corrosion is caused by inhibition treatment due to the formation of insoluble cerium oxide/hydroxide and aluminum oxide/hydroxide films on the surface. The film on the alloy surface appears to be formed by conglomeration of smaller particles of cerium, which are mostly crystalline as shown by earlier SEM studies (Ref 18). On exposing Al 6013-20SiC to cerium chloride, cathodic reactions proceed at the sites of intermetallic precipitates of copper in Al 6013-20 SiC and the solution becomes alkaline. It has been suggested that under conditions of high pH aluminum oxide is soluble and cerium oxide remains insoluble. The condition becomes favorable for the deposition of cerium oxide/hydroxide at the cathodic sites at the interface (Ref 18). The film of cerium oxide replaces the film of aluminum hydroxide on the surfaces with increased time of exposure as shown by earlier studies on Al 7075 (Ref 28-30). The above observation appears to be in agreement with our studies. Pitting was not observed in specimens treated with cerium chloride up to 70 °C; however, shallow pits were observed at 100 °C. Cerium chloride treatment stifles the cathodic reaction sites provided by the deposition of intermetallic precipitates, mainly by deposition on Cu at the Al/SiC interface. It has also been suggested that increasing alkalinity converts trivalent cerium to tetravalent cerium oxide /hydroxide films on cathodic sites and this explains the corrosion inhibition of Al 6013-20 SiC (p) composite where the major concern is the enhanced corrosion caused by the presence of precipitates like $CuAl_2$ at the Al/SiC interface. Studies on AA 2124 (Ref 33, 34) also showed that high concentration of Cu intermetallics at the SiC/Al interface were responsible for the preferential attack. Studies on the texture and kinetics of Ce_2O film are inconclusive and more microanalytical studies are required (Ref 32, 35). It has been, however, shown in the above study that cerium chloride satisfactorily inhibits the corrosion of Al 6013-20 SiC composites.

4. Conclusions

On the basis of the experimental evidence presented, the following conclusions are drawn

1. The corrosion rate of tempers -O, -F and -T4 of Al 6013-20 SiC (p) is effectively reduced by a potassium dichromate-sodium bicarbonate treatment.
2. Cerium chloride is highly effective in inhibiting the corrosion of O, F, and T4 tempers of Al 6013-20 SiC (p) in 3.5 wt.% NaCl at 25, 50, 70, and 100 °C.
3. Cerium chloride is an effective inhibitor and suppresses the cathodic reaction at the Al/SiC interface of Al 6013-20 SiC (p). It is more effective than sodium molybdate in chloride solutions.
4. Morphological evidence supports the formation of cerium oxide/hydroxide protective films, which inhibit the corrosion of Al 6013-20 SiC (p) alloy in different tempers.
5. Temper T4 of alloy 6013-20SiC shows a high resistance to localized corrosion.

Acknowledgment

The authors appreciate the support and encouragement provided by KFUPM in conducting the above investigations.

References

1. A.L. Geiger and J.A. Walker, The Processing and Properties of Discontinuously Reinforced Aluminum Composites, *JOM*, 1991, **39**, p 8
2. D.J. Lloyd, Particle Reinforced Aluminum and Magnesium Matrix Composites, *Int. Met. Rev.*, 1994, **39**(1), p 1
3. J.E. Hatch, *Aluminum Properties and Physical Metallurgy.* ASM, Metals Park, OH, 1990, p 27–32
4. B. Thanaboonsombut and T.H. Sanders Jr., The Effect of Cooling Rate from the Melt on the Recrystallization Behavior of Aluminum Alloy 6013, *Metall. Mater. Trans. A*, 1997, **28**, p 2137
5. R.A. Jenisiki, B. Thanaboorsombut, and T.H. Sanders Jr., The Effect of Iron and Manganese on the Recrystallization Behavior of Hot Rolled and Solution Heat Treated Aluminum Alloy 6013, *Metall. Mater. Trans. A*, 1996, **27**, p 19–27
6. N.J. Poole, D.J. Lloyd, and J.D. Embury, Effect of Natural Ageing on the Evolution of Yield Strength During Artifical Ageing for Al-Mg-Si-Cu Alloys, *Mater. Sci. Eng. A*, 1997, **234-236**, p 306
7. T.G. Nieh and D.J. Chellman, Modulus Measurement in Discontinuous Reinforced Aluminum Composite, *Scripta Metall.*, 1984, **18**, p 925
8. S.V. Nair, J.K. Tien, and R.C. Bartes, SiC-Reinforced Aluminum Metal Matrix Composites, *Int. Met. Rev.*, 1985, **30**(6), p 275
9. P.S. Gilman, Discontinuously Reinforced Aluminum. Ready for the 1990s, *J. Met.*, 1991, August, p 7
10. P.P. Trzaskoma, Pit Morphology of Aluminum Alloys and Silicon, *Corrosion*, 1990, **46**, p 402
11. D.M. Aylor and P.J. Moran, Effect of Reinforcement on the Pitting Behavior of Aluminum Based Metal Matrix Composites, *J. Electrochem. Soc.*, 1986, **133**, p 951

12. J.F. Mcyintyre, A.H. Le, S. Golledge, et al., *Corrosion Behavior of SiC Reinforced Aluminum Alloys, Report No. NW-SC-Tr87-36*. Naval Warfare Centre, Silver Springs, Marylan, Sept. 1987
13. Z. Ahmad and B.J. Abdul Aleem, Effect of Temper on Seawater Corrosion of an Aluminum-Silicon Composite Alloy, *Corrosion*, 1996, **52**(11), p 857
14. T.D. Burleigh, E. Ludwiczak, and R.A. Petri, Intergranular Corrosion of an Aluminum-Magnesium Silicon Copper Alloy, *Corrosion*, 1995, **5**, p 1
15. S. Lin, H. Greene, H. Shih, and F. Mansfeld, Corrosion Protection of Al/SiC Metal Matrix Composites by Anodizing, *Corrosion*, 1992, **48**(1), p 61
16. F. Mansfeld and S.L. Jean Jaquet, The Evaluation of Corrosion Protection Measurements for Metal Matrix Composites, *Corros. Sci.*, 1980, **26**(9), p 727
17. F. Mansfeld, S. Lin, S. Kim, and H. Shih, Chemical Protection of Al Alloys and Al Based Metal Matrix Composites, *Corrosion*, 1989, **45**(8), p 615
18. B.R.W. Hinton, D.R. Arnot, and N.E. Ryan, Cerium Conversion Coatings for the Corrosion Protection of Aluminum, *Mater. Forum*, 1986, **9**(3), p 162
19. A.J. Davenport, H.S. Isaacs, and M.W. Kendig, Xanes Investigation of the Role of Cerium Compounds as Corrosion Inhibitors for Aluminum, *Corros. Sci.*, 1991, **32**(516), p 653
20. F. Mansfeld, *Seawater Corrosion Test Program, Final Report Contract No. 00014-91-J-1041*. ONR Washington, Oct. 1, 1994
21. ASTM G31-72, *Standard Practice for Laboratory Immersion Corrosion Testing of Metals; in Annual Book of Standards*. ASTM, Philadelphia, PA, 1994
22. ASTM G5-87, *Standard Reference Method for Making Potentiostatic and Potentiodynamic Polarization Measurements, in Annual Book of Standards*. ASTM, Philadelphia, PA, 1993
23. ASTM G59-91, *Standard Practice for Conducting Potentiodynamic, Polarization Resistance Measurements, Annual Book of Standards*. ASTM, Philadelphia, PA, 1994
24. ASTM G61-78, *Standard Practice for Making Cyclic Polarization Measurements, in Annual Book of Standards*. ASTM, Philadelphia, PA, 1994
25. K.C. Goretta, W. Nu, J.L. Routbourt, and P.K. Rohtagi, Solid Particle Erosion of Aluminum Particulate Ceramic Particles Composites, *Proc. Cong. Tribology of Composite Materials*. Oakridge, TN, ASM Int., May 1-3, 1990, p 147–155
26. Z. Ahmad and B.J. Abdul Aleem, *The Erosion Corrosion of Al-SiC Composites in Seawater, Final Report, AR-14-65*. King Abdul Aziz City for Science and Technology, Riyadh, 1998
27. Z. Ahmad, P.T. Paulette, and B.J. Abdul Aleem, Mechanism of Localized Corrosion of Al 6013-20 SiC(p), *J. Mater. Sci.*, 2000, **35**, p 2573
28. M. Vogelsang, R.J. Arsenualt, and R.M. Fisher, In-situ HVEM Study of Dislocation Generation at Al/SiC Interfaces in Metal Matrix Composites, *Metall. Trans. A*, 1986, **17**, p 379
29. B.R.W. Hinton, D.R. Arnott, and N.E. Ryan, Electrochemical Formation of Aluminum Ceride on Aluminum, *Mater. Forum*, 1984, **7**, p 211
30. D.R. Arnott, B.R.W. Hinton, and N.E. Ryan, The Inhibition of Aluminum Alloy Corrosion by Cerous Cations, *Corrosion*, 1989, **45**, p 12–18
31. B.A. Shaw, G.D. Davis, T.L. Fritz, and K.A. Oliver, A Molybdate Treatment of Enhancing the Passivity of Aluminum in Chloride Containing Environment, *J. Electrochem. Soc.*, 1990, **137**(1), p 359
32. A.J. Davenport and H.S. Isacs, X-ray Absorption Study of Cerium in the Passive Film on Aluminum, *J. Electrochem. Soc.*, 1989, **136**(6), p 1837
33. Z. Ahmad and B.J. Abdul Aleem, Effect of Velocity and Elevated Temperatures on Pitting of Al 6013-20SiC (P) Composites in 3.5 wt.% NaCl, *Br. Corros. J.*, 1998, **33**(3), p 230
34. R.K. Conrad Mcintyre and S.L. Golledge, The Effect of Heat Treatment on the Pitting Behavior of SiC/AA 2124, *Corrosion*, 1990, **46**(11), p 902
35. F. Mansfeld and Y. Wang, *Chemically Induced Passivity of Aluminum Alloys and Aluminum Based Metal Matrix Composites, Final Report, Contract No: 0014-91-J-1041*. University of Southern California, 1995